RESEARCH
Open Access

Low-complexity interference variance estimation methods for coded multicarrier systems: application to SFN

Marius Caus[1*], Ana I Perez Neira[1,2] and Markku Renfors[3]

Abstract

For single-frequency network (SFN) transmission, the echoes coming from different transmitters are superimposed at the reception, giving rise to a frequency selective channel. Although multicarrier modulations lower the dispersion, the demodulated signal is sensitive to be degraded by inter-symbol interference (ISI) and inter-carrier interference (ICI). In view of this, we use channel coding in conjunction either with filter bank multicarrier (FBMC) modulation or with orthogonal frequency division multiplexing (OFDM). To deal with the loss of orthogonality, we have devised an interference-aware receiver that carries out a soft detection under the assumption that the residual interference plus noise (IN) term is Gaussian-distributed. To keep the complexity low, we propose to estimate the variance of the IN term by resorting to data-aided algorithms. Experimental results show that regardless of the method, FBMC provides a slightly better performance in terms of coded bit error rate than OFDM, while the spectral efficiency is increased when FBMC is considered.

1 Introduction

With the aim of making an efficient use of the spectrum, 3GPP has introduced the multimedia broadcast and multicast service (MBMS) for delivering multimedia content to mobile users [1]. Among the possible transmission schemes, we focus on single-frequency network (SFN), which has also been widely studied in the DVB-T digital TV context. In a SFN, the frequency reuse factor is one, and thus, the user equipment (UE) receives several delayed versions of the same signal, giving rise to an artificial multipath channel. In this regard, the use of the orthogonal frequency division multiplexing (OFDM) technique facilitates the implementation of the SFN concept. It must be mentioned that depending on the inter-site distance and the system parameters such as the sampling frequency and the subcarrier spacing, OFDM may not present a good balance between the resilience against multipath fading and the spectral efficiency. In other words, the minimum cyclic prefix (CP) length that is required to absorb

the last echo may lead to a dramatic spectral efficiency reduction. However, if the CP is not long enough to encompass the maximum channel excess delay, the demodulated signal will suffer from inter-symbol interference (ISI) and inter-carrier interference (ICI). To overcome the OFDM limitations, we can resort to the filter bank multicarrier (FBMC) modulation [2]. The FBMC technique is designed to achieve maximum bandwidth efficiency since no redundancy is transmitted in the form of a CP. Furthermore, the subcarrier signals follow the Nyquist pulse shaping idea, which makes the FBMC modulation more robust against narrow-band interferences and synchronization errors than OFDM. However, the channel is dispersive at the subcarrier level and thus the equalization is not a straightforward task; see, e.g., [3,4]. For further details about how OFDM and FBMC compare, we address the reader to [5].

To the best of the authors' knowledge, FBMC-based SFNs have not been considered in the literature earlier. In this work, we assume the worst case scenario in which orthogonality is not restored neither in OFDM nor FBMC cases. To combat the drawbacks of this definitely challenging scenario, OFDM and FBMC transmission are combined with channel coding. Bearing this in mind, we

*Correspondence: marius.caus@upc.edu
[1]Department of Signal Theory and Communications, Universitat Politecnica de Catalunya(UPC), Barcelona 08034, Spain
Full list of author information is available at the end of the article

propose mapping the received symbols into soft bits under the assumption that the residual interference plus noise (IN) is Gaussian-distributed. Simulation-based results show that the FBMC system is able to give the same or slightly better performance than OFDM in terms of bit error rate (BER) while the spectral efficiency significantly increases.

It is worth mentioning that previous works have compared coded FBMC and OFDM modulations in the presence of severe multipath fading [6-8]. These studies highlight the importance of characterizing the statistical information of the signal that corrupts the demodulated data. In this sense, we have formulated an analytical model for the additive noise and interference effects, as well as evaluated the complexity that is required to get a closed-form expression of its variance. The order of the complexity may render the solution impractical. Therefore, we opt to use low-complexity estimation methods for the variance of the IN term. In this work, we have described two data-assisted strategies. The complexity analysis reveals that the proposed methods alleviate the complexity with respect to the cost of implementing the ideal receiver, which perfectly characterizes the variance of the IN term.

In view of the above discussion, the contributions of this paper are summarized as follows:

- We evaluate the complexity and memory requirements of each variance estimator. In addition, the coded BER is assessed when each method is applied. The complexity costs and the system performance of the ideal receiver, which perfectly characterizes the variance of the IN term, are also provided. By confronting the ideal receiver with the receiver that relies on the variance estimation, we are able to provide insight into performance degradation when the complexity is reduced.
- We carry out a comparison between OFDM and FBMC in the context of SFN transmission. Regardless of which estimator is implemented, the numerical results reveal that FBMC slightly outperforms OFDM in terms of coded BER. In this sense, multi-tap equalization plays a key role in FBMC systems to improve link reliability especially in highly frequency-selective channels. This allows us to conclude that the FBMC modulation scheme is a potential candidate to be used in a SFN. To the best of our knowledge, FBMC has not been considered earlier in the literature for SFN.

The remainder of the paper is organized as follows. In Section 2, we describe the system model in a SFN. The loss of orthogonality in the FBMC context is studied in Section 3. Based on the analysis in Section 3, we design in Section 4 a receiver that is interference aware. To alleviate

the complexity, two data-assisted methods are investigated to estimate the variance of the IN term. Section 5 analyzes the complexity and the memory that is required to estimate the variance by each method. The coded BER is evaluated in Section 6 when the interference-aware receiver is applied in OFDM and FBMC systems. Finally, Section 7 draws the conclusions.

2 System model

In this work, we consider the SFN represented in Figure 1. Since the synchronization issues are out of the scope of this paper, we assume that all the transmitters are perfectly time- and frequency-synchronized. Nevertheless, the signals that come from the first- and second-order neighbors will give rise to an artificial multipath. More distant base stations (BSs) are ignored, so in the considered scenario, 19 BSs are transmitting in the same band.

Assuming that the UE is synchronized with the nearest BS, the received signal can be written as a function of the virtual channel as $r[n] = h_v[n] * s[n] + w[n]$, where

$$r[n] = \sum_{i=1}^{19} \frac{1}{\sqrt{L_i}} s[n - \tau_i] * h_i[n] + w[n]. \qquad (1)$$

Here $s[n]$ is the signal transmitted by all the BSs and $w[n]$ is the additive white Gaussian noise. The term τ_i stands for the delay of the ith transmitter with respect to the BS
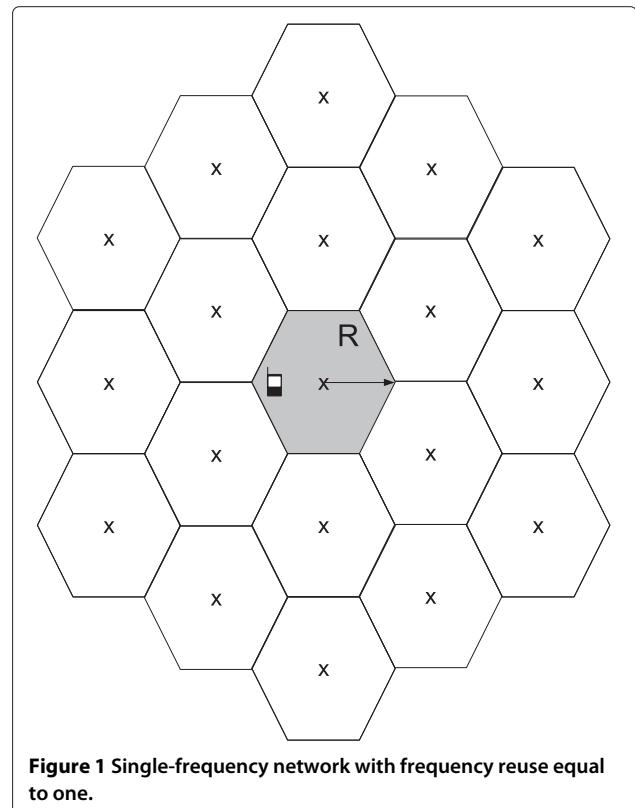

Figure 1 Single-frequency network with frequency reuse equal to one.

of reference, which can be identified without loss of generality with any index. The propagation conditions between the ith transmitter and the UE are modeled by the channel impulse response (CIR) $h_i[n]$ and by the combined effect of the path loss and the shadowing, which is expressed as $L_i(\text{dB}) = \bar{L}_i(\text{dB}) + X_i(\text{dB})$. The variable $X_i(\text{dB})$ accounts for the shadowing, and it follows a Gaussian distribution with zero mean and standard deviation σ_x. By contrast, $\bar{L}_i(\text{dB})$ is a distance-dependant term given by $\bar{L}_i(\text{dB}) = 128.1 + 37.6\log_{10}(d_i)$, where d_i denotes the distance to the ith transmitter in kilometers [9]. With the aim of studying the most general case, we consider that the UE receives several delayed versions of the signal broadcasted by a given transmitter. Therefore, $h_i[n]$ is modeled as a tapped delay line, which indicates that the channel between the receiver and any transmitter is frequency selective.

3 SFN based on FBMC transmission

This section aims at introducing the expressions for FBMC when the orthogonality is not restored in a SFN. The transmitted signal in the FBMC context is given by

$$s[n] = \sum_{k=-\infty}^{\infty} \sum_{m=0}^{M-1} f_m\left[n - k\frac{M}{2}\right] y_m[k] \tag{2}$$

$$f_m[n] = p[n]\, e^{j\frac{2\pi}{M}m\left(n - \frac{L-1}{2}\right)}, \tag{3}$$

where $p[n]$ is the prototype pulse, M is the number of subcarriers, and m is the subcarrier index. To avoid confusion, the sampling index n is used for the high-rate signals while the low-rate signals utilize the index k. Due to its good time and frequency localization properties, we opt to design the pulse as [10] details having fixed the length to $L = 4M$. The symbols $y_m[k]$ are generated according to the offset quadrature amplitude modulation (OQAM) scheme. Hence, they can be understood as real pulse amplitude modulation (PAM) symbols at double symbol rate and multiplied by a phase term, which is defined as follows:

$$\theta_m[k] = \begin{Bmatrix} 1 & m+k \ \text{even} \\ j & m+k \ \text{odd} \end{Bmatrix}. \tag{4}$$

Then $y_m[k] = d_m[k]\,\theta_m[k]$, where $d_m[k]$ is the real PAM symbol transmitted on the mth subcarrier. At the receiver side, the UE sees the transmitted signal through the corrupted version described in (1). To recover the information multiplexed on each subband, the received samples are fed into a bank of filters and then the outputs are downsampled to obtain the low-rate signals. The

output of the qth filter, i.e., $z_q[k] = \left(r[n] * f_q^*[-n]\right)_{\downarrow M/2}$, can be compactly formulated as

$$z_q[k] = \sum_{m=q-1}^{q+1} y_m[k] * g_{qm}[k] + w_q[k] \tag{5}$$

with

$$g_{qm}[k] = \left(f_m[n] * h_v[n] * f_q^*[-n]\right)_{\downarrow M/2} \tag{6}$$

$$w_q[k] = \left(w[n] * f_q^*[-n]\right)_{\downarrow M/2}. \tag{7}$$

The operation $(.)_{\downarrow x}$ performs a decimation by a factor of x. Expression (5) indicates that symbols are degraded by ISI and ICI. Thanks to the good spectral confinement of the pulses, ICI mainly comes from the adjacent subbands. In addition, the equivalent channel impulse responses $\{g_{qm}[k]\}$ are assumed different from zero for $-2 \le k \le 2$. The energy of the interference terms corresponding to $|k| \ge 3$ can be neglected. To draw an analogy with OFDM, we formulate the demodulated data in a matrix way. Stacking the outputs of the analysis filter bank, we obtain

$$\mathbf{z}[k] = [z_0[k] \ldots z_{M-1}[k]]^T = \sum_{t=-2}^{2} \mathbf{G}[t]\,\mathbf{y}[k-t] + \mathbf{w}[k] \tag{8}$$

where

$$\mathbf{y}[k] = [\theta_0[k]\,d_0[\,k] \ldots \theta_{M-1}[k]\,d_{M-1}[k]]^T \tag{9}$$

$$\mathbf{w}[k] = [w_0[k] \ldots w_{M-1}[k]]^T. \tag{10}$$

The matrix $\mathbf{G}[t]$ accommodates the coupling between carriers at the tth time instant. The element located at the mth row and lth column is given by

$$[\mathbf{G}[t]]_{ml} = \begin{Bmatrix} g_{ml}[t] & \text{if } l \in S_m \\ 0 & \text{otherwise} \end{Bmatrix}, 0 \le m, l \le M-1, \tag{11}$$

where $S_m = \{\text{mod}_M(m-1), m, \text{mod}_M(m+1)\}$ contains three indexes. Note that $\text{mod}_M(x)$ accounts for the modulus M of x.

Considering briefly the OFDM system model when the orthogonality is destroyed, the vector at the FFT output reads as

$$\mathbf{z}[k] = \mathbf{H}[0]\,\mathbf{y}[k] + \mathbf{H}[1]\,\mathbf{y}[k-1] + \mathbf{w}[k]. \tag{12}$$

Now the vector $\mathbf{y}[k]$ contains complex QAM symbols. The closed-form expression of $\mathbf{H}[0], \mathbf{H}[1] \in \mathbb{C}^{M \times M}$ can be found in [11]. The matrix formulation written in (12) highlights that only the previous block induces ISI. The reason lies in the fact that there is no time overlapping when OFDM is considered. Conversely, the prototype pulse

used in the FBMC case exhibits better frequency localization properties than the sinc-like shape. As a consequence, the matrices $\mathbf{H}[0]$, $\mathbf{H}[1]$ are not so sparse as $\{\mathbf{G}[t]\}$.

To combat the frequency selectivity of the channel in FBMC systems, it is customary to apply a multi-tap subcarrier equalizer. Since the orthogonal properties are satisfied in the real field, we extract the real part of the equalizer output after compensating the phase term. Based on that and denoting by $b_q[k]$ the equalizer used in the qth subband, which is designed according to the zero-forcing criterion [3], the symbol estimation can be expressed as

$$\check{d}_q[k] = \frac{\Re\left(\theta_q^*[k]\left(b_q[k] * z_q[k]\right)\right)}{h_q} = d_q[k] + i_q[k] \tag{13}$$

$$h_q = \Re\left(\sum_{l=-L_b}^{L_b} g_{qq}[-l]\, b_q[l]\right). \tag{14}$$

It is worth mentioning that $b_q[k]$ is different from zero for $-L_b \le k \le L_b$, thus h_q corresponds to the term that weighs the desired symbol after being equalized. Expanding (13), we differentiate between desired and undesired information. The additive IN term $i_q[k]$ includes contributions of ICI, ISI, and noise. The closed-form expression is given by

$$i_q[k] = \frac{1}{h_q}\sum_{\substack{m=q-1\\m\neq q}}^{q+1}\sum_{t=-L_b-2}^{L_b+2}\Re\left(\theta_q^*[k]\,\theta_m[k-t]\,\mathbf{b}_q^T\mathbf{g}_{qm}[t]\right)$$
$$\times\, d_m[k-t]$$
$$+ \frac{1}{h_q}\sum_{\substack{t=-L_b-2\\t\neq 0}}^{L_b+2}\Re\left(\theta_q^*[k]\,\theta_q[k-t]\,\mathbf{b}_q^T\mathbf{g}_{qq}[t]\right)$$
$$\times\, d_q[k-t] + \frac{1}{h_q}\Re\left(\theta_q^*[k]\,\mathbf{b}_q^T\mathbf{w}_q[k]\right), \tag{15}$$

where $\mathbf{b}_q = \left[b_q[-L_b]\cdots b_q[L_b]\right]^T$, $\mathbf{g}_{qm}[t] = \left[g_{qm}[t+L_b]\cdots g_{qm}[t-L_b]\right]^T$, and the noise vector is $\mathbf{w}_q[k] = [w_q[k+L_b]\cdots w_q[k-L_b]]^T$. Since the OFDM modulation has been widely studied, we refrain from formulating the IN term in the OFDM context. Its expression can be computed as [11] details.

4 Interference-aware receiver

Bearing in mind the system model described in Section 3, we devise a technique to decode the received message in the presence of ISI, ICI, and noise. To protect the information from the detrimental effects caused by the artificial multipath fading, the bits are encoded by means of a parallel concatenated coding scheme, which consists of two identical systematic encoders, the transfer function of which is $G(D) = \left[1, \frac{1+D^2+D^3}{1+D+D^3}\right]$. Next the coded bits are mapped as Figure 2 illustrates. Finally, the sequence of symbols is fed to the synthesis filter bank (SFB), which is in charge of frequency multiplexing the symbols. The symbol mapper and the synthesis filter bank stages will be different depending on the multicarrier modulation to be used.

At the receiver, the analysis filter bank (AFB) enables demodulating the information that is conveyed on each subband. The equalization stage, which is designed under the zero-forcing criterion for both OFDM and FBMC systems, is appended at the analysis filter bank output. At this point, the soft detection can be performed from the output of the equalizers. Bearing in mind (13), the *a posteriori* log-likelihood ratios (LLRs) of the encoded bits c_l, for $l = 1,\ldots,b$, can be simplified using the Max-Log approximation as follows:

$$\text{LLR}\left(c_l|\check{d}_q[k]\right) = \frac{\min\limits_{d:c_l=0}\left|\check{d}_q[k]-d\right|^2 - \min\limits_{d:c_l=1}\left|\check{d}_q[k]-d\right|^2}{2\sigma_q^2} \tag{16}$$

where b is the number of bits that constitutes the PAM symbols. The expression $d : c_l = 1$ ($d : c_l = 0$) defines the set of symbols whose lth bit is 1 (0). It is worth emphasizing that we have assumed that the bits are equiprobable and the interference plus noise term is a real-valued random variable that is Gaussian-distributed, i.e., $i_q[k] \sim \mathcal{N}(0,\sigma_q^2)$. The same approach is followed in [8]. Note that the mean of the IN term is always zero. Under the assumption that symbols have zero mean, we can infer from (15) that $\mathbb{E}\left\{i_q[k]\right\} = 0$ if

$$\mathbb{E}\left\{\Re\left(\theta_q^*[k]\,\mathbf{b}_q^T\mathbf{w}_q[k]\right)\right\} = \sum_{l=-L_b}^{L_b}\Re\left(\theta_q^*[k]\,b_q[l]\right)\mathbb{E}\left\{\Re\left(w_q[k-l]\right)\right\}$$

$$- \Im\left(\theta_q^*[k]\,b_q[l]\right)\mathbb{E}\left\{\Im\left(w_q[k-l]\right)\right\} = 0, \tag{17}$$
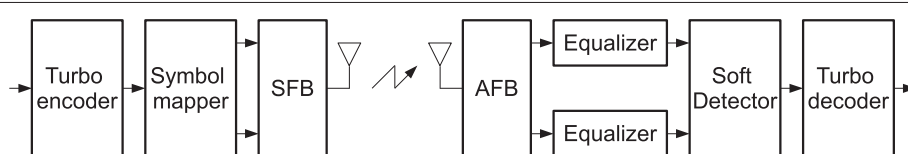

Figure 2 Transmitter and receiver block diagram.

which can be proven by demonstrating that $\mathbb{E}\{\Re\left(w_q[k-l]\right)\} = \mathbb{E}\{\Im\left(w_q[k-l]\right)\} = 0$. To this end, we expand $\mathbb{E}\{\Re\left(w_q[k-l]\right)\}$ and $\mathbb{E}\{\Im\left(w_q[k-l]\right)\}$ as follows:

$$
\mathbb{E}\{\Re\left(w_q[k-l]\right)\} = \sum_{n=-L+1}^{0} \Re\left(f_q[-n]\right)\mathbb{E}\{\Re\left(w\left[(k-l)\tfrac{M}{2}-n\right]\right)\} \\
+ \Im\left(f_q[-n]\right)\mathbb{E}\{\Im\left(w\left[(k-l)\tfrac{M}{2}-n\right]\right)\}
$$
(18)

$$
\mathbb{E}\{\Im\left(w_q[k-l]\right)\} = \sum_{n=-L+1}^{0} \Re\left(f_q[-n]\right)\mathbb{E}\{\Im\left(w\left[(k-l)\tfrac{M}{2}-n\right]\right)\} \\
- \Im\left(f_q[-n]\right)\mathbb{E}\{\Re\left(w\left[(k-l)\tfrac{M}{2}-n\right]\right)\}.
$$
(19)

Since $w[n]$ is modeled as a complex circularly symmetric Gaussian variable with mean 0 and variance N_0, then $\mathbb{E}\{\Re\left(w[n]\right)\} = \mathbb{E}\{\Im\left(w[n]\right)\} = \mathbb{E}\{\Re\left(w[n]\right)\Im\left(w[n]\right)\} = 0$. From this definition, it follows that (18) and (19) are zero. With that we conclude the proof that demonstrates that $\mathbb{E}\{i_q[k]\} = 0$.

If the statistical information of the noise and the symbols, as well as the instantaneous channel, is perfectly known, it is possible to formulate σ_q^2 in a closed-form expression as follows:

$$
\sigma_q^2 = \mathbb{E}\left\{\left|i_q[k]\right|^2\right\} = \frac{1}{|h_q|^2}\mathbb{E}\left\{\left(\Re\left(\theta_q^*[k]\mathbf{b}_q^T\mathbf{w}_q[k]\right)\right)^2\right\} \\
+ \frac{E_s}{2|h_q|^2}\sum_{\substack{m=q-1 \\ m\neq q}}^{q+1}\sum_{t=-L_b-2}^{L_b+2}\left(\Re\left(\theta_q^*[k]\theta_m[k-t]\mathbf{b}_q^T\mathbf{g}_{qm}[t]\right)\right)^2 \\
+ \frac{E_s}{2|h_q|^2}\sum_{\substack{t=-L_b-2 \\ t\neq 0}}^{L_b+2}\left(\Re\left(\theta_q^*[k]\theta_q[k-t]\mathbf{b}_q^T\mathbf{g}_{qq}[t]\right)\right)^2.
$$
(20)

We have assumed that the symbols are zero-mean, independent, and uncorrelated with the noise, i.e., $\mathbb{E}\{d_m[k]d_q[n]\} = \frac{E_s}{2}\delta_{m,q}\delta_{k,n}$ and $\mathbb{E}\{d_m[k]w_q[n]\} = 0$, $\forall m, q, k, n$. The factor 2 highlights that the PAM symbols are obtained after staggering in-phase and quadrature components of QAM symbols whose variance is E_s. Regarding the filtered noise, the analytical expression of its variance can be found in [4,12]. Based on (20) we should first calculate the coefficients $\{g_{qm}[k]\}$, which are given by

$$
g_{qm}[k] = \sum_{t=0}^{L_v-1} h_v[t]e^{j\pi qk}\alpha_{qm}^k[t]e^{-j\frac{2\pi}{M}qt}
$$
(21)

$$
\alpha_{qm}^k[t] = \sum_{v=0}^{L-1} p[v]p\left[v+t-k\frac{M}{2}\right]e^{j\frac{2\pi}{M}(m-q)\left(v-\frac{L-1}{2}\right)},
$$
(22)

where L_v is the maximum channel excess delay of the virtual channel. Even knowing $\left\{e^{j\pi qk}\alpha_{qm}^k[t]\right\}$ beforehand, it can be deduced from (21) that the complexity cost in terms of multiplications is $2L_v$. Taking into account which values of $g_{qm}[k]$ are different from zero, the total number of operations is approximately $30L_vM$. According to the expressions provided in [11], the complexity in the OFDM case is in the order of M^3. From the perspective of reducing the complexity, we propose to estimate the power using two different methods.

4.1 Direct decision method

The first method to estimate (20) consists in computing the empirical expectation of $i_q[k]$ over a period, T, in which the channel conditions do not substantially vary. The estimation boils down to compute the following expression

$$
\check{\sigma}_q^2 = \frac{1}{T}\sum_{k=0}^{T-1}\left|i_q[k]\right|^2.
$$
(23)

It can be readily verified that the complexity required to compute (23) is substantially reduced with respect to that required to obtain the theoretical expression of (20). In order to get the instantaneous value of the IN term, it is mandatory to subtract the data symbols from the equalized signals, i.e., $i_q[k] = \check{d}_q[k] - d_q[k]$. To perfectly compute the term $i_q[k]$, the receiver needs to know the transmitted data beforehand. Hence, this method relies on the transmission of T pilot sequences in the form of a preamble. Nevertheless, this may imply transmitting longer training sequences than those exclusively used for channel estimation and synchronization purposes, which would decrease the spectral efficiency. To overcome this drawback, the method proposed in this section refrains from using pilots. As a consequence, the IN term is approximated to $\check{i}_q[k] = \check{d}_q[k] - s_q^0[k]$, where $s_q^0[k]$ is an estimation of $d_q[k]$. It must be mentioned that the reliability of the proposed estimator crucially relies on the decisions made from the equalized signals. If the decisions are not correct, the variance estimation will substantially deviate from the real value. In this sense, the simplest option consists in detecting symbols according to the maximum likelihood (ML) criterion, which yields this estimator

$$
\check{\sigma}_{q,0}^2 = \frac{1}{T}\sum_{k=0}^{T-1}\min_{s_q^0[k]\in\mathbb{X}}\left|\check{d}_q[k]-s_q^0[k]\right|^2,
$$
(24)

where $\mathbb{X}$ is the modulation alphabet. One way to evaluate the quality of the estimator is to check if it is unbiased. To this end, we calculate the conditional expectation of $\check{\sigma}_{q,0}^2$ given that the event $\left\{s_q^0[0]\ldots s_q^0[T-1]\right\}$, where $s_q^0[k]$,

$k = 0, \ldots, T - 1$, is any symbol of the constellation diagram. That is, $s_q^0[k] \in \mathbb{X}$ for $0 \leq k \leq T - 1$. Taking into account that symbols are zero-mean and independent, we can write the expectation in this form

$$
\begin{aligned}
\mathbb{E}\left\{\check{\sigma}_{q,0}^2 | s_q^0[0] \ldots s_q^0[T-1]\right\} &= \frac{1}{T} \sum_{k=0}^{T-1} \mathbb{E}\left\{\left|d_q[k] - s_q^0[k]\right|^2\right\} \\
&\quad + \mathbb{E}\left\{\left|i_q[k]\right|^2\right\} \\
&= \frac{1}{T} \sum_{k=0}^{T-1} \mathbb{E}\left\{\left|d_q[k] - s_q^0[k]\right|^2\right\} \\
&\quad + \sigma_q^2.
\end{aligned}
$$

(25)

Unless the decisions are correct, i.e., $d_q[k] = s_q^0[k]$, the estimator will be biased as (25) shows. This highlights the importance of regenerating the message as accurately as possible.

4.2 Refined direct decision method

We have empirically observed that the estimator derived in Section 4.1 gives satisfactory results when the modulation order is low, e.g., 2PAM. On the contrary, for higher-order modulations, the BER curves exhibit an error floor. To remedy this, it is clear that the estimator has to be refined. In this sense, the approach that we have followed is based on regenerating the sequence of transmitted symbols from the outputs of the turbo decoder. That is, already detected bits from the initial iteration are fed into the turbo encoder stage and then the coded bits are mapped to obtain the OQAM symbols. From Figure 3 it can be inferred that the refined estimation is equivalent to

$$
\check{\sigma}_{q,1}^2 = \frac{1}{T} \sum_{k=0}^{T-1} \left|\check{d}_q[k] - s_q^1[k]\right|^2.
$$

(26)

Notice that the extrinsic LLRs computed by the first turbo decoder are not directly forwarded to the second turbo decoder to be used as *a priori* information. That is because the term $\check{\sigma}_{q,0}^2$, which is computed as (24) specifies, may excessively deviate from the real value. If so, errors

will propagate on subsequent turbo iterations since the decoding algorithms are sensitive to the variance errors. It is also important to remark that, contrary to [13], the estimated symbols are not used to cancel out the interferences but to get a more accurate estimation of the transmitted symbols when compared to the approach followed in Section 4.1. As (25) indicates, the lower the symbol error rate is, the lower is the bias. The reason why we have discarded canceling out the interferences has to do with the complexity burden that is required to calculate the coefficients of the equivalent channels $\{g_{qm}[k]\}$.

It is worth mentioning that the symbols in FBMC systems are modulated at a rate twice that of the symbols in OFDM. Hence, for a fixed window, the number of symbols that are used to calculate (23), (24), and (26) will be $T/2$ in the OFDM case.

5 Comparison of different estimation techniques

In this section, we compare the two estimators described in Section 4. In this sense, the Table 1 summarizes the order of the complexity and the memory that is approximately required by each method. The analysis that has been conducted to get the values of Table 1 is detailed hereinafter.

5.1 DDM

The direct decision method relies on performing an exhaustive search over all the elements of the modulation alphabet as (24) highlights. Provided that b bits are used to represent any point of the constellation diagram, then the number of norms that has to be calculated is equal to $2^b TM$. On the positive side, the approach followed in Section 4.1 does not need to store any data.

5.2 RDDM

The complexity required to implement the refined direct decision method is tantamount to computing the complexity of the grey blocks in Figure 3. Towards this end, we first analyze $\check{\sigma}_{q,0}^2$. According to (24), the number of norms to be computed is $2^b TM$, where b is the number
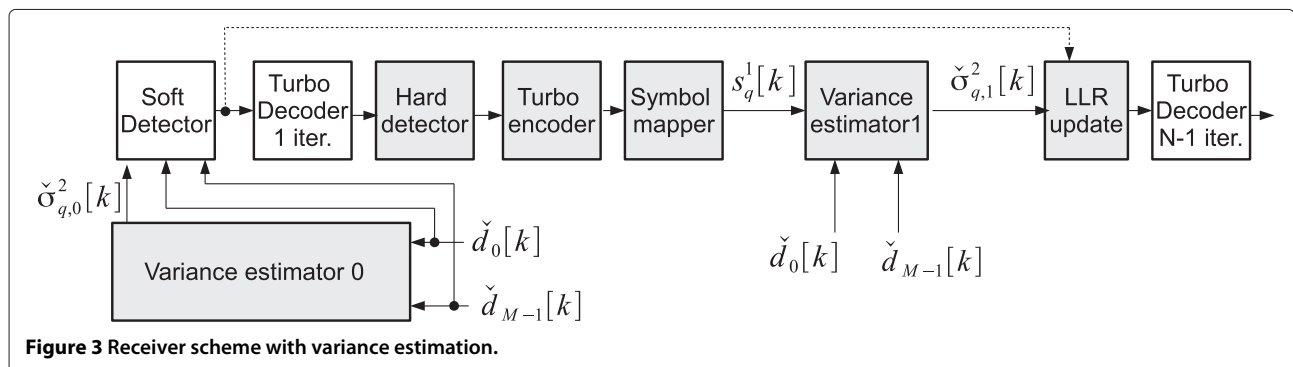

Figure 3 Receiver scheme with variance estimation.

Table 1 Complexity order and memory requirements of computing the variance of the IN term in all the subcarriers

Estimation method	Complexity order	Memory
DDM	$2^b TM$	-
RDDM	$TM\left(2^b + 3b + 4\right)$	TM

DDM, direct decision method; RDDM, refined direct decision method.

of bits that constitutes the symbols. The next process that contributes to the increase of complexity is the conversion from soft bits to binary data. Considering that a single mapping only takes one operation together with the fact that the code rate is set to $r_{\text{code}} = 1/3$ implies performing $\frac{b}{3}TM$ operations. Then each bit has to be coded again by concatenating two identical systematic convolutional codes. Then it follows that the turbo code computes $\frac{2b}{3}TM$ coded bits, and each one is obtained after performing four logical operations. To regenerate the message, the coded bits are mapped into OQAM symbols by performing MT look-up operations. As (26) indicates, the refined estimation requires computing MT norms. In the last step, we multiply LLR($c_l|\check{d}_q[k]$) by $\frac{\check{\sigma}_{q,0}^2}{\check{\sigma}_{q,1}^2}$, which takes TM divisions and TM multiplications. According to the values gathered in Table 1, the complexity costs when $b = 2$ results approximately in $14TM$ operations. Bearing in mind the complexity analysis conducted in Section 4, the number of operations to get the exact value of $\left\{\sigma_q^2\right\}$ is in the order of M^3 and $30L_\nu M$ when the OFDM and the FBMC modulation scheme is considered, respectively. This highlights that although the strategy devised in Section 4.2 is the most complex, the method is still interesting because there is a good prospect of L_ν and M^2 being higher than T. Therefore, the refined direct decision method is likely to be more efficient than the computation of the real variance. Unlike what happens in the DDM, the regenerated message has to be stored so that it can be loaded later on to estimate the variance. As a result, there should be enough available memory to save TM symbols.

A feature that is common to all the algorithms described in Section 4 is that they do not operate in real time. That is, the variance is estimated after receiving T consecutive multicarrier symbols and storing the decision variables $\left\{\check{d}_q[k]\right\}$ for $0 \le k \le T - 1$ and $0 \le q \le M - 1$. This observation reveals that in addition to the memory requirements that are summarized in Table 1, the receiver has to reserve some additional space to save TM equalized symbols.

6 Numerical results

In this section, we compare OFDM and FBMC in the SFN scenario depicted in Figure 1 where the cell radius is equal

to $R = 1$ km. Hence, the user is confined in the coverage area of a single transmitter while the exact position randomly varies for each channel realization. Regarding the system parameters, the 10-MHz bandwidth is split into $M = 1,024$ subbands, out of which 600 are active. The carrier frequency is 2 GHz and the sampling frequency is set to 15.36 MHz. The power delay profile of $\{h_i[n]\}$ obeys the ITU Vehicular A (VehA) or the ITU Vehicular B (VehB) models, and we assume that the channel is invariant for $T = 20$ consecutive FBMC symbols or, equivalently, for $T = 10$ consecutive OFDM symbols. The shadowing standard deviation is $\sigma_x = 8$ dB. As for the decoder, we employ the MAX-LOG-MAP algorithm with $N = 4$ iterations. The symbols belong to 16-QAM, which means that the real symbols $\{d_q[k]\}$ are 4-PAM. The assessment has been made in terms of BER against the energy bit-to-noise ratio (E_b/N_0), which is defined as

$$E_b/N_0 = \left(\sum_{i=1}^{19}\frac{1}{L_i}\right)\frac{E_s\left(\frac{M+CP}{M}\right)}{4r_{\text{code}}N_0},\tag{27}$$

where the noise samples are generated as follows $w[n] \sim \mathcal{CN}(0, N_0)$ and E_s is the symbol energy. The constant 4 accounts for the number of bits that constitutes the 16-QAM symbols. It is worth mentioning that $CP = 0$ for FBMC systems and $CP = \frac{M}{4}$ in the OFDM case.

Notice that the receiver described in Section 4 takes for granted that the residual IN term is Gaussian-distributed. To determine if this assumption yields a mismatch modeling, we have examined the Gaussianity of $i_q[k]$ in the FBMC case. Towards this end, we plot in Figure 4 the theoretical probability density function (PDF) of $i_q[k]$ for a given channel realization on subcarrier $q = 410$, provided that the IN term was characterized by this statistical information $i_q[k] \sim \mathcal{N}(0, \sigma_q^2)$. To verify that this supposition is accurate, the PDF is confronted with the histogram. To get the histogram we generate several realizations of $i_q[k]$ for $q = 410$ using the formula in (15). In other words, we fix the channel so that it coincides with the realization employed to obtain the theoretical PDF, and then the symbols and the noise are independently generated to get the samples of $i_q[k]$. It is obvious that if noise dominates over the interference, the working hypothesis is true. Thus, we can state that the most critical case is when the magnitude of the noise and that of the interference are in the same order. Bearing this mind, we have generated the taps of $h_i[n]$ according to the ITU Vehicular B channel model. Regarding the receiver processing, the equalizers perform a single-tap filtering, i.e., $L_b = 0$. As Figure 4 shows, the histogram fits the outline of the PDF well. Note that good matching is observed at high and low noise regimes. For the sake of brevity, we have only included the plots corresponding to $q = 410$, but similar results have been observed on
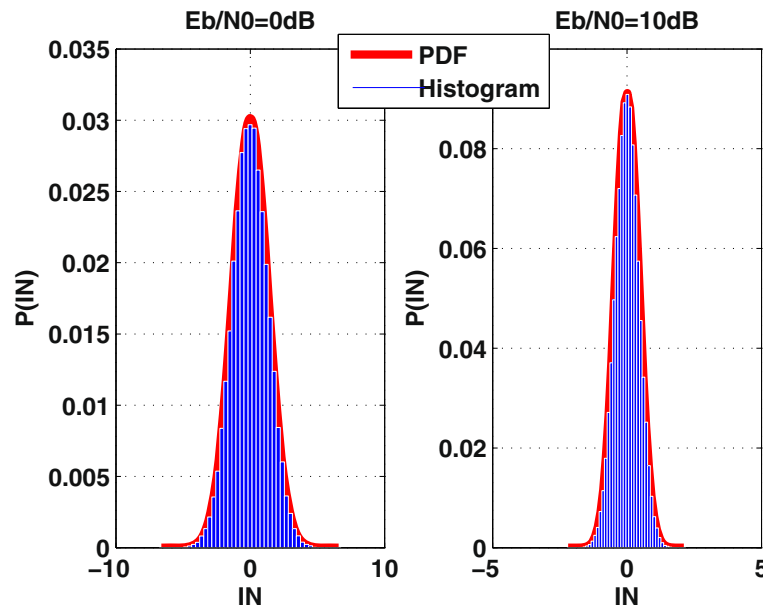
Figure 4 Probability density function and histogram of $i_q[k]$ for $q = 410$. The propagation conditions obey the VehB channel model.

different subcarriers. Based on this, we have assumed that the Gaussian approximation holds true when detecting the symbols.

6.1 Benchmark

Before evaluating the impact of variance estimation methods described in Section 4, we depict in Figure 5 the BER curves when the variance of $i_q[k]$ is perfectly estimated. When the power delay profile of the channel obeys the ITU Vehicular A model, the FBMC system does not benefit from performing a multi-tap equalization because the

channel frequency response at the subcarrier level is practically flat. With the parameters used in this scenario, the maximum channel excess delay satisfies $L_v \leq 216$, and therefore, the demodulated signals are free of ISI when OFDM is considered. The improvement of FBMC with respect to OFDM for $\frac{E_b}{N_0} \leq 14$ dB is a consequence of the energy wastage that implies the CP transmission.

In Figure 6, we asses the system performance when the channel is modeled according to the ITU Vehicular B model. Now the gap between the multi-tap and single-tap linear equalization is widened. The reason lies in the fact
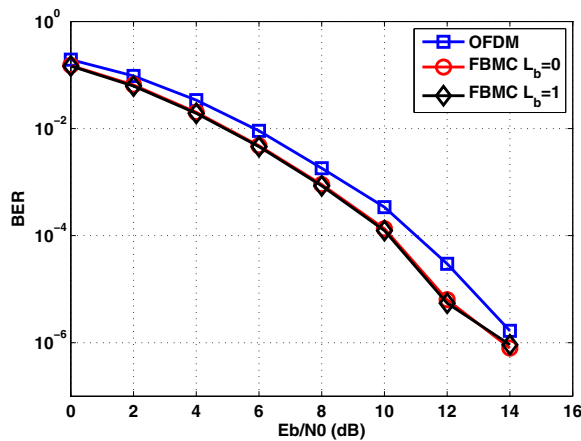
Figure 5 BER versus $\frac{E_b}{N_0}$ when the receiver is based on perfect IN variance estimation. The propagation conditions obey the VehA channel model.
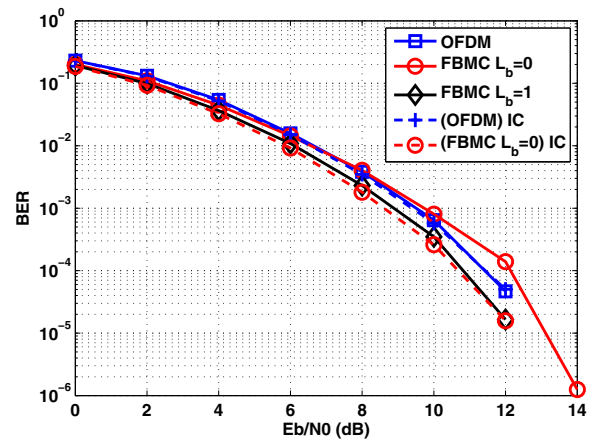

Figure 6 BER versus $\frac{E_b}{N_0}$ when the receiver is based on either perfect IN variance estimation or perfect interference cancelation. The propagation conditions obey the VehB channel model.

that the channel coherence bandwidth has reduced since the maximum channel excess delay is upper bounded as follows $L_\nu \leq 484$. As a result, the transmission based on the OFDM technique does not succeed in avoiding inter-block interference (IBI). By setting $CP = \frac{M}{4}$, the IBI is reduced to a higher extend but not enough to give better performance than the FBMC modulation that equalizes the channel with three taps per subband. These results reveal that it is of paramount importance to mitigate the residual interference as much as possible. This observation has motivated us to test one alternative receiver that performs a perfect interference cancelation (IC). That is, we get rid of the interference from vectors (12) and (13) before they are fed into the channel decoding stage. Then, the noise is the only source of interference. The curves in Figure 6 indicate that the improvement brought by the perfect IC is marginal. As it is pointed out in Section 4, the complexity required to estimate the interference may be too high, which provides further arguments in favor of the receiver that is based on estimating the variance.

To further justify the results provided in Figure 6, we have pictured in Figure 7 the noise-to-interference ratio (NIR) averaged over all subcarriers. Borrowing the notation from (20), the metric in the FBMC case is given by

$$\text{NIR} = \frac{1}{600} \sum_{q \in S_a} \frac{\mathbb{E}\left\{ \left(\Re \left(\theta_q^*[k] \, \mathbf{b}_q^T \mathbf{w}_q[k] \right) \right)^2 \right\}}{\frac{E_s}{2} \sum_{(m,t) \neq (q,0)} \left(\Re \left(\theta_q^*[k] \, \theta_m[k-t] \, \mathbf{b}_q^T \mathbf{g}_{qm}[t] \right) \right)^2},$$
(28)

where S_a contains the indices of those subcarriers that are active. Figure 7 confirms that multi-tap equalization removes the interference more effectively than the
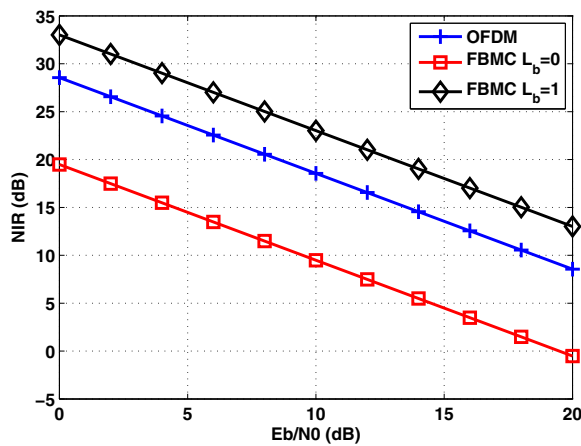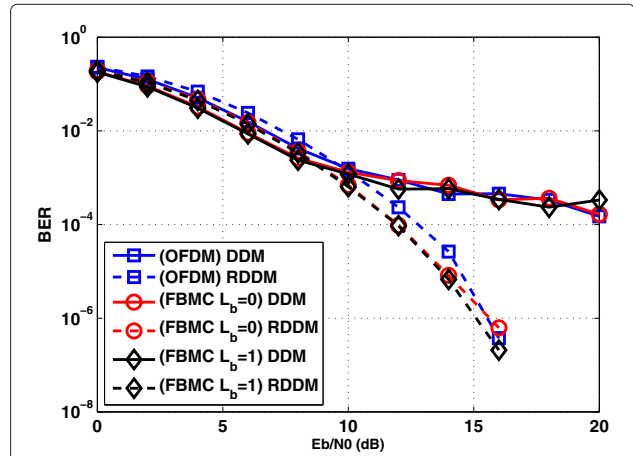

Figure 8 BER versus $\frac{E_b}{N_0}$ when the receiver implements different IN variance estimation methods for the VehA channel model.

single-tap counterpart in high-frequency selective channels. Hence, the results of Figure 7 are in accordance with the coded BER versus $\frac{E_b}{N_0}$ curves.

Regarding bandwidth efficiency, the spectral efficiency reaches 1.20 bits/s/Hz for the FBMC case. The OFDM counterpart results in 0.96 bits/s/Hz.

6.2 Evaluation of the proposed interference-aware receiver

In this section, we evaluate the performance of the receiver based on the variance estimation. The window used by all the methods described in Section 4 encompasses 20 FBMC symbols or, equivalently, 10 OFDM symbols. Figures 8 and 9 highlight that the plots obtained when the RDDM is applied are shifted to the right when compared to Figures 5 and 6. That is because the turbo decoder performs three iterations instead of four. As Figure 3 shows,
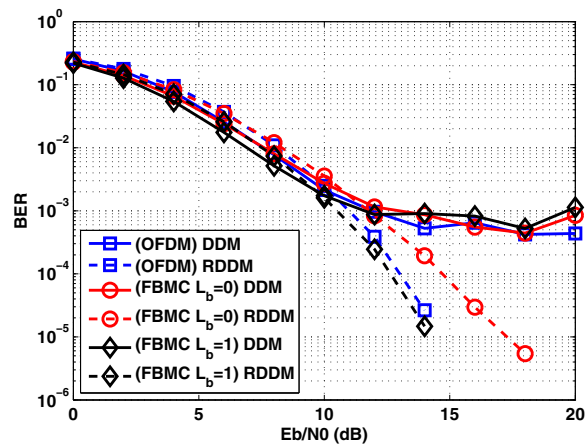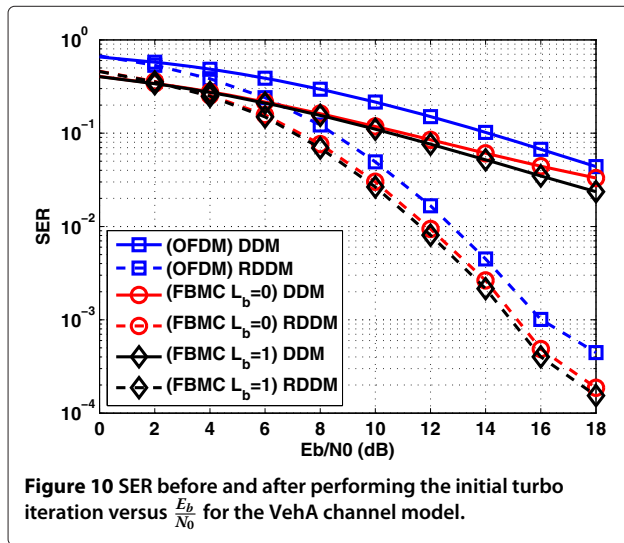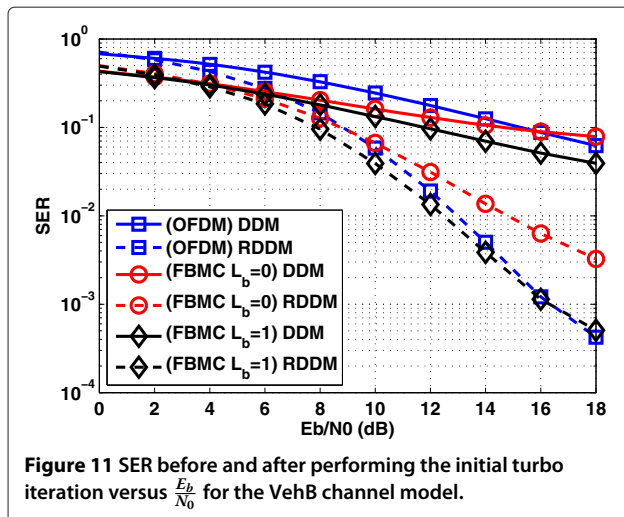

Figure 7 Average NIR versus $\frac{E_b}{N_0}$. The propagation conditions obey the VehB channel model.

Figure 9 BER versus $\frac{E_b}{N_0}$ when the receiver implements different IN variance estimation methods for the VehB channel model.

Figure 10 SER before and after performing the initial turbo iteration versus $\frac{E_b}{N_0}$ for the VehA channel model.

one iteration is devoted to estimating the variance. Recalling (25), we can assert that the degradation is also related to the errors committed when performing the symbol mapping after re-encoding the bits obtained at the output of the initial turbo iteration. By examining Figure 9, we can conclude that the degradation in FBMC systems is between 1 and 2 dB when the equalizers perform a multi-tap filtering. In the single-tap case, the degradation is substantially higher. Taking into consideration Figure 7, it seems that the cause is related to the insufficient interference mitigation capabilities exhibited by single-tap equalization in severe propagation conditions. In order to improve the performance, the interference has to be more effectively rejected. Notice that the curves associated with the receiver based on the DDM exhibit an error floor. The reason is that the tentative decisions used in (24) are too erroneous.

Figure 11 SER before and after performing the initial turbo iteration versus $\frac{E_b}{N_0}$ for the VehB channel model.

To support the results of Figures 8 and 9, we plot in Figures 10 and 11 the symbol error rate (SER) that is observed when the transmitted data is estimated according to the procedure followed by the DDM and the RDDM. Since the decoding algorithms are sensitive to the variance deviations, the coded BER performance relies on the accuracy with which the transmitted message is regenerated as (25) demonstrates. The results of Figures 10 and 11 can be understood as the evaluation of the SER at the input and the output of the initial turbo iteration. In Figure 10, the plots associated with the RDDM are equal or less than 1 dB apart. Hence, all the techniques suffer a similar deterioration for estimating the variance as Figure 8 shows. By contrast, when the selectivity of the channel becomes stronger as it happens in the scenario simulated with Vehicular B channel in Figure 9, the FBMC modulation combined with the single-tap zero forcing equalizer does not achieve competitive results when the variance is estimated. By observing Figure 11, it becomes clear that the degradation is related to the increased SER, which causes less reliable estimation. As it has been previously pointed out, the tentative decisions made when the DDM is applied are not reliable. This is confirmed in Figures 10 and 11.

7 Conclusions

In the worst case scenario, in the context of OFDM and FBMC, orthogonality is destroyed in a SFN. Based on this and taking into account that both schemes are combined with channel coding, we have devised an interference-aware receiver, which relies on the knowledge of the statistics of the IN term. When the residual interference is perfectly characterized, the OFDM technique and the FBMC modulation based on single-tap equalization perform reasonably close regardless of the channel. Therefore, we may opt to use the same single-tap equalizer both in OFDM and FBMC systems, resulting in a similar performance in terms of BER. To alleviate the complexity we propose two different data-assisted methods to estimate the variance of the IN term. The complexity analysis reveals that the RDDM is more complex than the DDM. The simulation-based results demonstrate that the additional complexity is well justified because the receiver based on the RDDM achieves the lowest coded BER. When the RDDM is considered under severe multipath fading, it becomes important to use multi-tap equalization in FBMC systems. Anyway, it is enough to use three-tap subcarrier equalizers, which leads to relatively minor increase in the overall computational complexity. With proper multi-tap equalization, FBMC is able to reach or slightly exceed the error performance of CP-OFDM while supporting about 25% higher data rate.

Author details

[1]Department of Signal Theory and Communications, Universitat Politecnica de Catalunya(UPC), Barcelona 08034, Spain. [2]Centre Tecnologic de Telecomunicacions de Catalunya (CTTC), Castelldefels, Barcelona 08860, Spain. [3]Department of Electronics and Communications Engineering, Tampere University of Technology, Tampere 33101, Finland.

References

1. ETSI 3rd Generation Partnership Project (3GPP), 3GPP TS 25346, Introduction of the multimedia broadcast multicast service (MBMS) in the radio access network (RAN). stage 2 (release 11) (2012)
2. P Siohan, C Siclet, N Lacaille, Analysis and design of OFDM/OQAM systems based on filterbank theory. Signal Process. IEEE Trans. **50**(5), 1170–1183 (2002)
3. T Ihalainen, TH Stitz, M Rinne, M Renfors, Channel equalization in filter bank based multicarrier modulation for wireless communications. EURASIP J. Appl. Signal Process. **2007**, 049389 (2007)
4. D Waldhauser, L Baltar, J Nossek, in *IEEE 9th Workshop on Signal Processing Advances in Wireless Communications, 2008. SPAWC 2008*. MMSE subcarrier equalization for filter bank based multicarrier systems (IEEE, 2008), pp. 525–529
5. B Farhang-Boroujeny, OFDM versus filter bank multicarrier. Signal Process. Mag. IEEE **28**(3), 92–112 (2011)
6. T Ihalainen, T Stitz, A Viholainen, M Renfors, in *Proceedings of the IEEE International Symposium on Circuits and Systems, 2006. ISCAS 2006* Performance comparison of LDPC-coded FBMC and CP-OFDM in beyond 3G context (IEEE, 2006), pp. 21–24
7. G Ndo, P Siohan, M Hamon, in *2010 IEEE 72nd Vehicular Technology Conference Fall (VTC 2010-Fall)* A comparison between coded OFDM/OQAM and CP-OFDM modulations over multipath channels (IEEE, 2010), pp. 1–5
8. G Ndo, P Siohan, MH Hamon, in *2010 International Conference on Advanced Technologies for Communications (ATC)* Performances of coded OFDM/OQAM over PLC impaired by impulsive and colored noise (IEEE, 2010), pp. 1–6
9. International Telecommunication Union, in *Recommendation ITU-R M.1225* Guidelines for the evaluation of radio transmission technologies for IMT-2000 (ITU, 1997)
10. M Bellanger, in *2001 IEEE International Conference on Acoustics, Speech, and Signal Processing, 2001. Proceedings. (ICASSP '01)*. vol. 4 Specification and design of a prototype filter for filter bank based multicarrier transmission (IEEE, 2001), pp. 2417–2420
11. X Sun, Q Wang, L Cimini, L Greenstein, D Chan, ICI/ISI-aware beamforming for MIMO-OFDM wireless systems. Wireless Commun. IEEE Trans. **11**, 378–385 (2012)
12. M Caus, Transmitter-receiver designs for highly frequency selective channels in MIMO FBMC systems. Signal Process. IEEE Trans. **60**(12), 6519–6532 (2012)
13. R Zakaria, D Le Ruyet, in *2011 IEEE 22nd International Symposium on Personal Indoor and Mobile Radio Communications (PIMRC)* On spatial data multiplexing over coded filter-bank multicarrier with ML detection (IEEE, 2011), pp. 1391–1395